THE JOURNAL OF PHYSICAL CHEMISTRY C

ARTICLE

pubs.acs.org/JPCC

Nitrogen-Doped Hollow Carbon Nanoparticles with Excellent Oxygen Reduction Performances and Their Electrocatalytic Kinetics

Guixiang Ma,[†,‡] Rongrong Jia,[†,‡] Jianghong Zhao,[*,†] Zhijian Wang,[†] Chang Song,[†,‡] Suping Jia,[†] and Zhenping Zhu[*,†]

[†]State Key Laboratory of Coal Conversion, Institute of Coal Chemistry, Chinese Academy of Sciences, Taiyuan 030001, China

[‡]Graduate University of Chinese Academy of Sciences, Beijing 100049, China

ABSTRACT: To propel the commercialization of fuel cells, the development of efficient nonprecious metal catalysts, specifically cathodic oxygen reduction catalysts, is turning into reality because the great advancements have been made on nitrogen-doped carbon materials recently. In this study, we demonstrated that nitrogen-doped hollow carbon nanoparticles (N-HCNPs) exhibit excellent electrocatalytic performance for oxygen reduction reaction (ORR) in alkaline fuel cells. Cyclic voltammetry and rotating ring-disk electrode voltammetry showed that the ORR activity of N-HCNPs approaches that of commercial Pt−C catalyst and is much better compared with nitrogen-free counterparts due to the incorporation of nitrogen atoms into graphitic structures. Kinetic studies indicated that the involvement of nitrogen induces a totally different oxygen adsorption mechanism and a four-electron dominated reaction pathway for N-HCNPs in comparison with nitrogen-free HCNPs, very similar to the observations in Pt−C. Moreover, N-HCNPs exhibited good operation stability and excellent tolerance to methanol crossover and CO poisoning for ORR superior to that of Pt−C. Our findings suggest that N-HCNPs catalyst is a promising alternative for the Pt-based catalysts in fuel cells.

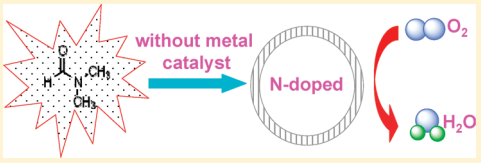

1. INTRODUCTION

As the energy crisis becomes increasingly severe, the fuel cell—an efficient power generation source with high efficiency and low emission—will make a significant contribution in the utilization of energy in the near future.[1,2] In a fuel cell, the cathodic oxygen reduction reaction (ORR) rate is slower by six-fold than the oxidation reaction rate of the anode. This makes ORR one of the critical factors limiting the performance of fuel cells[1,3] so that the development of efficient ORR catalysts plays a key role in the practical application of fuel cells. To date, platinum-based materials are the most widely used electrocatalysts for ORR. However, the problems of durability, scarcity, and high cost of Pt significantly hamper the commercial application of fuel cells. In the past few decades, intensive efforts have been to reduce Pt usage or replace it completely. Non-noble metal catalysts involving transition-metal alloy[4] and transition-metal macrocyclic compounds[5,6] have been developed. More importantly, researchers recently found that nitrogen-doped carbon nanostructures, including nitrogen-doped carbon nanotubes (CNTs),[2,3,7−13] graphene sheets,[14] and graphitic arrays,[15] exhibit excellent electrocatalytic performance for ORR. However, whether the inclusion of nitrogen atoms into carbon structures really improves ORR is still under debate because nitrogen-doped carbon materials previously employed were usually synthesized with metal catalysts whose residues often enhanced ORR activity. Therefore, metal-free catalysts are required to clarify the impact of nitrogen-doping.

Herein we report the excellent electrocatalytic ORR performance of nitrogen-doped hollow carbon nanoparticles (N-HCNPs) synthesized via a simple one-pot method utilizing detonation-assisted chemical vapor deposition (DCVD) of dimethylformamide (DMF) devoid of metal catalysts.[16] It is the first time that N-HCNPs act as an efficient catalyst for ORR without the involvement of any metals. The effect of nitrogen-doping was investigated by comparing the catalytic activity of N-HCNPs and nitrogen-free HCNPs. Furthermore, the electrocatalytic kinetics of N-HCNPs for ORR was studied.

2. EXPERIMENTAL METHODS

2.1. Synthesis of N-HCNPs and HCNPs. Both N-HCNPs and HCNPs were synthesized using the DCVD technique with 2,4,6-trinitrophenol (TNP) as explosive. Experiments were performed in a sealed stainless-steel pressure vessel (14 cm^3) equipped with a pressure gauge. Detonation was initiated by quick heating (20 °C min^{-1}) to 320 °C (the ignition temperature of TNP), then a high-temperature and high-pressure environment of ∼1000 °C and 20−45 MPa was created inside the vessel. After detonation, the vessel was cooled in air to ambient temperature, after which the gaseous product was vented and the solid product was collected. For HCNPs synthesis, a ternary mixture of TNP, phenol, and cobalt acetate with a desired ratio was employed, and hierarchical carbon nanoparticles with mesoporous cores and microporous shells (CSCNPs) were first produced. Then, the CSCNPs were treated with oxidative 1.5 M HNO_3 and refluxed for 12 h to remove catalysts and mesopore walls in their cores

Received: August 26, 2011
Revised: November 2, 2011
Published: November 08, 2011

while simultaneously retaining the carbon shells. After that the suspension was filtered, washed with deionized water and ethanol, and dried overnight, producing HCNPs without metal impurities.[17] N-HCNPs were obtained using a binary mixture of TNP and DMF without involving any metal catalysts.[16] It is very important for the evaluation of the intrinsic catalytic function of N-HCNPs and the relevant mechanisms to exclude completely the possible effects of metal on ORR catalysis. N-HCNPs products were repeatedly washed with deionized water and ethanol, then filtered, dried overnight, and stored for future use in electrochemical tests.

2.2. Characterization. Transmission electron microscopy (TEM) was performed using a JEM-2010 TEM operated at 200 kV. Elemental compositions and chemical bonds were investigated via X-ray photoelectron spectroscopy (XPS), which was performed using a Thermo ESCALAB 250 spectrometer employing an Al Kα X-ray source with a 500 μm electron beam spot.

2.3. Evaluation of Electrocatalytic Activity. Electrochemical measurements were carried out using a computer-controlled potentiostat (CHI 760D, CH Instrument) equipped with a typical three-electrode cell and a gas flow system. Electrocatalytic activity was evaluated using cyclic voltammetry (CV) and rotating ring disk electrode (RRDE) voltammetry. CV and RRDE were collected in 0.1 M KOH electrolyte. A platinum wire and an Ag/AgCl electrode were employed as counter and reference electrodes, respectively. The working electrode was prepared as follows: 5 mg of N-HCNPs, 50 μL of Nafion solution (5 wt %), and 1 mL of ethanol were mixed and sonicated to form a uniform, well-dispersed catalyst ink, after which 10 μL of the ink solution was carefully deposited on a circular glassy carbon (GC) electrode and air-dried with an infrared lamp before measurement. All potentials reported in this study were referenced to that of the Ag/AgCl electrode. For CV measurements, the working electrode was first scanned between −1.2 and 0.2 V at a sweep rate of 100 mV/s for 20 cycles after the electrolyte was saturated with pure oxygen for at least 0.5 h. Then, the steady CV of the working electrode was recorded at a sweep rate of 100 mv/s between −1.2 and 0.2 V at room temperature. The ORR polarization curve was obtained in the oxygen-saturated KOH solution between 0.2 and −1.0 V at a sweep rate of 10 mV/s, whereas the Pt ring potential was set at 0.5 V. To remove the capacitive current of the working electrode, the background current was measured by running the above sweep profile in Ar-purged KOH electrolyte after ORR measurements and was subtracted from the ORR polarization curve. Therefore, the net Faradic current of ORR was obtained for evaluation of ORR activity. For comparison, nitrogen-free HCNPs and commercial Pt−C (20% Pt on Vulcan XC-72R, Johnson Matthey) electrodes were prepared and used as described above. Activity of the HCNPs and the Pt−C catalysts were also tested using CV and RRDE.

3. RESULTS AND DISCUSSION

The morphology and structure of N-HCNPs and HCNPs were observed using TEM (Figure 1). Both N-HCNPs and HCNPs displayed core−shell structures with entirely hollow cavities encapsulated by 2−5 nm thick carbon shells (Figure 1a,c). High-resolution TEM images in Figure 1b,d shows that N-HCNPs possess crystallized graphitic structure, similar to that previously reported,[16] and the shell structure of HCNPs is very analogous to that of N-HCNPs.

To analyze the elemental composition and investigate the binding configurations of nitrogen atoms in N-HCNPs, we

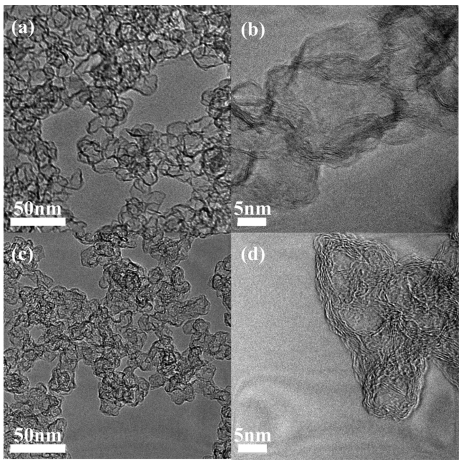

Figure 1. TEM images of (a,b) N-HCNPs and (c,d) HCNPs.

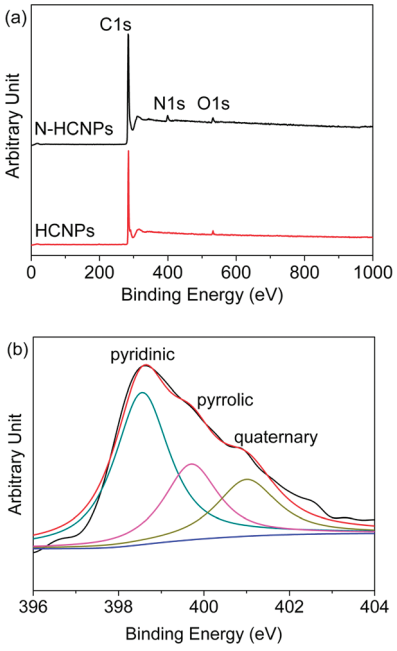

Figure 2. (a) XPS survey spectrum of N-HCNPs and HCNPs and (b) deconvoluted N1s XPS spectrum of N-HCNPs.

carried out XPS measurements with HCNPs for comparison. As shown in Figure 2a, the XPS survey spectrum of N-HCNPs shows a dominant narrow graphitic C 1s peak at 284 eV, an N 1s peak at ∼400 eV, and a weak O 1s peak at 531 eV. These clearly demonstrate the successful incorporation of nitrogen atoms within the graphitic structure of N-HCNPs. The nitrogen content of N-HCNPs was calculated to be ca. 4 atom %. In contrast, the XPS survey spectrum of HCNPs shows only two peaks at 284 and 531 eV belonging to C 1s and O 1s photoelectron excitation, respectively. The presence of an O 1s peak presumably arose from oxygen-containing species, as in the case of most nitrogen-doped carbon materials.[18] The high-resolution N 1s XPS spectrum, together with the curve deconvolution given in Figure 2b, reveals the presence of three peaks at binding energies of 398.6, 399.8, and 401 eV, corresponding to the pyridinic-, pyrrolic-, and quaternary-like nitrogen bonding configurations, respectively. Obviously, the pyridinic-like nitrogen is dominant in N-HCNPs.

dx.doi.org/10.1021/jp208257r |J. Phys. Chem. C 2011, 115, 25148–25154

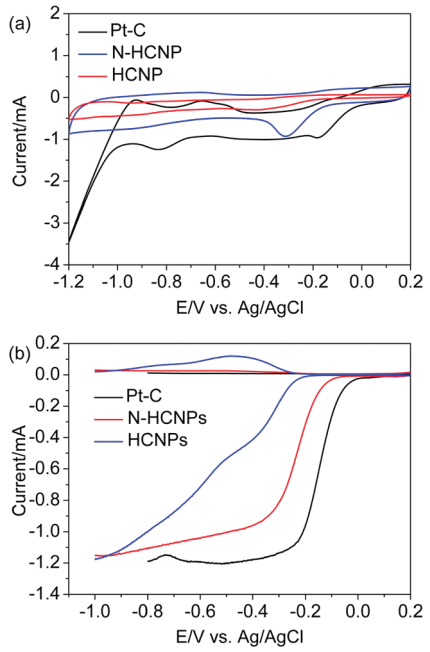

Figure 3. (a) CVs for ORR in oxygen-saturated 0.1 M KOH solution at a scan rate of 100 mV s^{-1}. (b) RRDE voltammetry in oxygen-saturated 0.1 M KOH solution at a scan rate of 10 mV s^{-1} after background subtraction. Electrode rotation speed was 1500 rpm and Pt ring electrode was held at 0.5 V.

However, there are still controversies about the real active-catalytic sites for ORR and the real role of nitrogen in enhancing ORR activity. Therefore, determining the nitrogen configurations responsible for the excellent ORR catalytic activity of N-HCNPs is very difficult, although some experimental and computational studies revealed that the pyridinic- or quaternary-like nitrogen groups could account for ORR electrochemical performance.[9,15,19−21] Deeper and more systematic studies are urgently needed to solve the obstacle for large-scale application of nonprecious nitrogen-doped carbon materials in ORR and fuel cells.

The electrocatalytic activity of N-HCNPs for ORR was investigated and compared with that of HCNPs and Pt−C catalysts by CV in 0.1 M KOH electrolyte saturated with O_2. A well-defined peak corresponding to the oxygen reduction current was observed at about −0.3 V for the N-HCNPs catalyst, approaching that of the Pt−C catalyst whose oxygen reduction peak appeared at about −0.18 V (Figure 3a). Although the nitrogen-free HCNPs catalyst also exhibited ORR catalytic activity to some extent with an oxygen reduction peak at around −0.45 V, the peak potential of the N-HCNPs catalyst is 0.15 V positive than that of nitrogen-free HCNPs. Results suggest significantly improved ORR activity with N-HCNPs compared with nitrogen-free HCNPs. Obviously, the nitrogen atoms in N-HCNPs lead to excellent ORR activity that approximates the performance of commercial Pt−C catalyst and is much better than that of nitrogen-free HCNPs.

ORR involves multielectron reactions that proceed mainly through the following possible pathways: a four-electron pathway (direct or indirect) to reduce molecular oxygen into water and a two-electron pathway to reduce O_2 into hydrogen peroxide ion (HO_2^-). To gain deeper insight into the ORR electrochemical process, RRDE voltammetry for N-HCNPs, HCNPs, and Pt−C catalysts was carried out in oxygen-saturated 0.1 M KOH electrolyte at a rotation speed of 1500 rpm, and HO_2^- formed during the reduction process was oxidized and detected by a Pt ring electrode at the potential of 0.50 V. Figure 3b shows the steady-state voltammograms of the three catalysts and the corresponding amperometric responses for the oxidation of HO_2^-. On the disk electrode, the steady-state voltammogram of Pt−C catalyst shows a typical polarization curve with a single, steep reduction wave and a mixed kinetic-diffusion control region (−0.25 to 0.1 V) above a flat diffusion-limited current plateau in the potential region of −0.7 to −0.3 V, suggesting a four-electron process. The voltammetric profile of N-HCNPs is similar to that of Pt−C catalyst, although the limiting current plateau is not as well-developed as the one obtained for Pt−C. Results indicate that ORR occurred mainly via a four-electron pathway on the N-HCNPs catalyst. In contrast, the polarization curve of nitrogen-free HCNPs exhibited an obvious two-step process with the onset potentials of about −0.22 and −0.55 V for the first and second reduction waves, respectively. Along with the substantial concomitant oxidation current at the ring electrode corresponding to HO_2^- production, this result indicates that oxygen reduction on HCNPs catalyst favors a two-electron pathway. The onset potentials and the currents at −0.4 V (1500 rpm) of N-HCNPs, HCNPs, and Pt−C catalysts are summarized in Table 1. The onset potential of N-HCNPs (−0.08 V) is 90 mV more negative than that of the Pt−C catalyst (0.01 V). The onset potential for the first reduction wave of HCNPs is much more negative (by 140 millivolts) compared with that of N-HCNPs. With respect to the ORR rate, the currents of N-HCNPs, HCNPs, and Pt−C at −0.4 V were selected, and the values are 0.96, 0.41, and 1.18 mA, respectively. This indicates that faster reduction rates (higher currents) can be expected on N-HCNPs and Pt−C catalysts at a lower ORR overpotential. The above results further exhibit that the ORR activity of N-HCNPs approaches that of the Pt−C catalyst and is superior to that of nitrogen-free HCNPs.

Table 1. Summary of the Important Performance Parameters of ORR Catalysts

	onset potential (V)	current (mA, at −0.4 V, 1500 rpm)	no. of electrons transferred (at −0.4 V, 1500 rpm)	H_2O selectivity (%, at −0.4 V, 1500 rpm)
Pt−C	0.01	1.18	3.88	94
N-HCNPs	−0.08	0.96	3.70	85
HCNPs	−0.22	0.41	2.26	13

We calculated the transferred electron number per oxygen molecule (n) during ORR and the H_2O selectivity using the following equations

$$n = \frac{4I_D}{I_D + \frac{I_R}{N}} \quad (1)$$

$$\text{selectivity}_{H_2O} = \frac{I_D - \frac{I_R}{N}}{I_D + \frac{I_R}{N}} \times 100 = \frac{n-2}{2} \times 100 \quad (2)$$

where I_D, I_R, and $N = 0.37$ are the disk current, ring current, and collection efficiency given by the manufacturer, respectively. Results (Table 1) calculated using the ring and disk currents

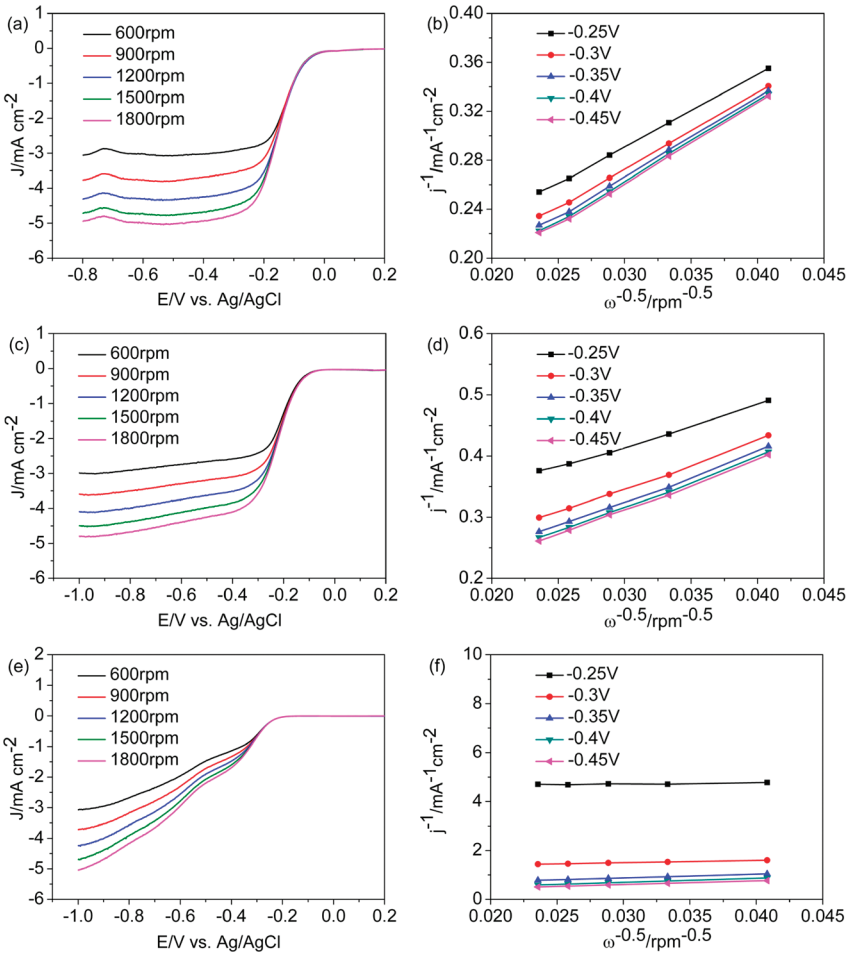

Figure 4. Polarization curves at different potentials and K−L plots of (a,b) Pt−C, (c,d) N-HCNPs, and (e,f) HCNPs.

show that ORR on N-HCNPs occurs by a 3.70 electron reaction at −0.4 V to produce ∼85% H_2O, indicating that an efficient four-electron pathway is the dominant reaction mechanism during the electrochemical process. The behavior of N-HCNPs is similar to that of the Pt−C catalyst, whose number of electrons transferred is 3.88 and with 94% H_2O product. In contrast, nitrogen-free HCNPs showed a two-electron pathway with 2.26 electrons transferred and only 13% H_2O selectivity. These findings further confirm that N-HCNPs possess excellent ORR activity.

For investigation of the possible reasons for the excellent ORR activity of N-HCNPs, it is essential to study the ORR kinetics on the catalysts. The ORR performance of N-HCNPs in the diffusion and kinetically limited region can be investigated using the Koutecky−Levich (K−L) equations (eqs 3 and 4)[22]

$$\frac{1}{j} = \frac{1}{j_k} + \frac{1}{B\omega^{0.5}} \tag{3}$$

$$B = 0.62nFC_{O_2}(D_{O_2})^{2/3}\nu^{-1/6} \tag{4}$$

where j is the measured current density, j_k is the kinetic-limiting current density, B is Levich slope, ω is the rotation speed, n is the overall number of electrons transferred in ORR, F is the Faraday constant, C_{O_2} is the bulk concentration of O_2 in the electrolyte, D_{O_2} is the diffusion coefficient of O_2, and ν is the kinematic viscosity of the electrolyte.

The ORR polarization curves of the catalysts at different rotation speeds and the K−L plots are presented in Figure 4. The K−L plots (j^{-1} vs $\omega^{-0.5}$) at various potentials exhibit good linearity and parallelism for N-HCNPs, HCNPs, and Pt−C catalysts, indicating first-order reaction kinetics for ORR with respect to the concentration of dissolved oxygen.[23,24] By extrapolation of linear K−L lines to the origin of the plots as ω approaches ∞, the kinetic-limiting current densities defined as the current densities in the absence of any mass transfer effects at different potentials were obtained by calculating the inverse of the Y intercept. This is an intrinsic kinetics analysis. Table 2 shows that the kinetic-limiting current densities of N-HCNPs at various potentials are about four times greater than that of nitrogen-free HCNPs and approximate that of the commercial Pt−C catalyst. Compared with nitrogen-free HCNPs, the superior electrocatalytic ORR activity of N-HCNPs can be attributed to their intrinsic property rather than oxygen diffusion. Together with the metal-free characteristics, the intrinsic property of N-HCNPs for ORR can be attributed exclusively to the incorporation of nitrogen atoms into the graphitic structure, suggesting that nitrogen-doping plays an important role in the ORR process of carbon catalysts.

Tafel analysis was also performed to gain information about the oxygen adsorption mechanism on N-HCNPs, HCNPs, and

dx.doi.org/10.1021/jp208257r |J. Phys. Chem. C 2011, 115, 25148–25154

Table 2. Kinetic Limiting Current Densities of N-HCNPs, HCNPs, and Pt−C at Different Potentials

potential E (V vs Ag/AgCl)	Pt−C $\lvert j_k \rvert$ (mA cm^{-2})	N-HCNPs $\lvert j_k \rvert$ (mA cm^{-2})	HCNPs $\lvert j_k \rvert$ (mA cm^{-2})
−0.3	6.25	4.56	0.79
−0.35	11.83	8.95	1.57
−0.4	15.94	12.25	2.79

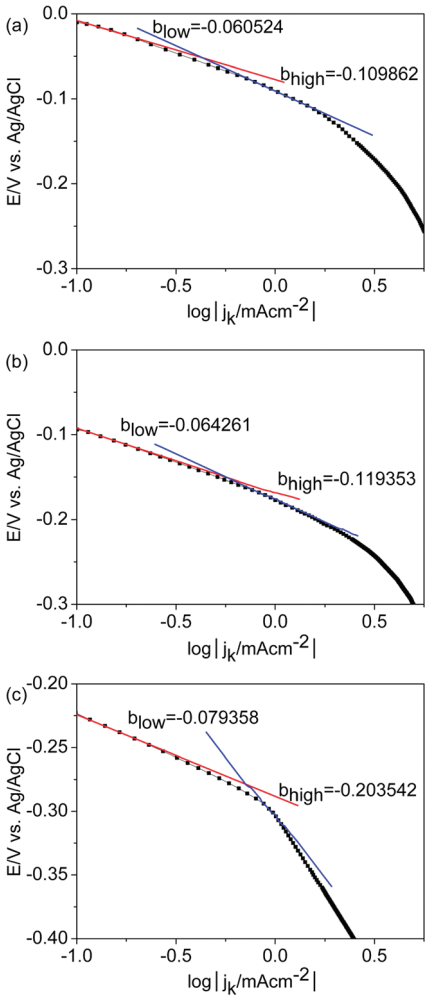

Figure 5. Diffusion-corrected Tafel plots of (a) Pt−C, (b) N-HCNPs, and (c) HCNPs data obtained from Figure 4 at 1500 rpm.

Pt−C catalysts. Diffusion-corrected Tafel plots were employed to eliminate the impact of diffusion on the adsorption kinetic analysis by plotting the potentials (E) as a function of the absolute values of the kinetic currents ($\lvert j_k \rvert$) in a semilogarithmic form (Figure 5). As reported by previous studies,[25,26] two distinct Tafel slopes in low and high current density regions (often from −1.2 to −0.7 and −0.4 to 0.1 on the log scale, respectively) were obtained on Tafel plots of Pt−C, N-HCNPs, and HCNPs. The Tafel slopes in low and high current density regions of Pt−C catalyst are −0.060524 and −0.109862 V dec^{-1}, respectively, which are close to the usually reported values for ORR on Pt electrode.[27,28] In theory, a Tafel slope of about −120 mV/dec indicates that the first electron transfer is the rate-determining step. The presence of two slopes suggests a switch between

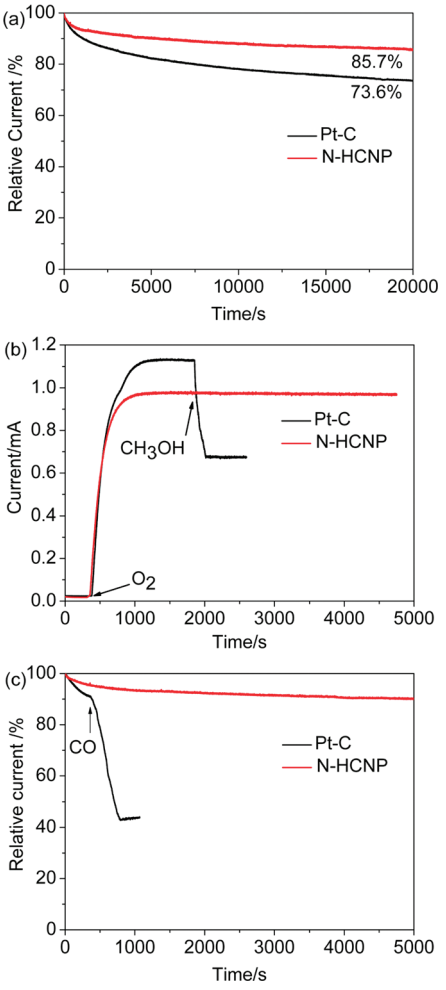

Figure 6. $i-t$ chronoamperometric response of N-HCNPs/GC and Pt−C/GC electrodes: (a) at −0.35 V in O_2 saturated 0.1 M KOH solution at a rotation rate of 1500 rpm; (b) when 3 M methanol was introduced at ∼1700 s under the same condition as panel a; and (c) when 10% (v/v) CO was introduced at ∼500 s under the same condition as panel a.

Temkin adsorption and Langmuir adsorption of oxygen on the Pt catalyst.[26] The Tafel slopes of N-HCNPs were calculated to be −0.064261 and −0.119353 V dec^{-1} in low and high current density regions and are very close to the values of Pt−C catalyst. This demonstrates that the oxygen adsorption mechanism of N-HCNPs is similar to that of Pt−C catalyst. For nitrogen-free HCNPs, the Tafel slope values of −0.079358 and −0.203542 V dec^{-1} in low and high current density regions were significantly different from that of N-HCNPs and Pt−C catalysts. This indicates that nitrogen-free HCNPs have greatly different oxygen adsorption mechanism compared with the other two catalysts. A high Tafel slope (absolute value) reveals that overpotential increases quickly with current density, leading to inferior ORR activity. Therefore, a low Tafel slope is desirable. The Tafel slopes of the three catalysts further indicate that N-HCNPs have excellent ORR activity approaching that of Pt−C catalyst and superior to that of nitrogen-free HCNPs.

Previous studies have concluded that the interaction between $^3O_2$ and carbon materials is a weak physisorption without charge transfer.[29−32] In contrast, theory calculations by Hu et al.[33]

suggested that $^3O_2$ absorption on the surface of nitrogen-doped carbon is energy-favorable and there is an accompanying electronic transition of O_2 with the adsorption process, because nitrogen-doping changes the charge density of carbon atoms adjacent to the nitrogen dopants. Thus, nitrogen-doping facilitates the adsorption and activation of O_2 on carbon materials. Moreover, theoretical results also showed that oxygen dissociation is facilitated on carbon atoms neighboring a nitrogen dopant, since the dissociation barrier and the activation barrier are reduced.[34] Along with these previous reports, we speculated that the excellent electrocatalytic activity of N-HCNPs compared with that of nitrogen-free HCNPs can be attributed to the lower O_2 adsorption and activation energy resulting from nitrogen-doping.

In addition to catalyst activity, stability and tolerance to crossover and poison effects are also critical issues in fuel cell application. To investigate the stability of N-HCNPs for ORR, we held the catalysts at −0.35 V for 20 000 s in 0.1 M KOH solution saturated with oxygen at a rotation rate of 1500 rpm. The corresponding *i*−*t* chronoamperometric responses of N-HCNPs and Pt−C are shown in Figure 6a. For N-HCNPs, a high relative current of 85.7% was preserved even after operation for 20 000 s, whereas the relative current of Pt−C catalyst decreased to 73.6%. This indicates that the stability of N-HCNPs is much better than that of the commercial Pt−C catalyst.

For direct methanol fuel cells, the crossover effect of methanol permeating through the membrane from anode to cathode can cause serious performance degradation by competitive electrooxidation of methanol. Both N-HCNPs and Pt−C electrodes were exposed to methanol to investigate their selectivity for ORR against methanol electrooxidation. As shown in Figure 6b, *i*−*t* chronoamperometric response of Pt−C catalyst exhibits a large current decrease after the addition of 3.0 M methanol, suggesting that Pt−C is active for methanol electrooxidation and is very sensitive to the methanol crossover effect. Remarkably, N-HCNPs showed excellent selectivity for ORR without any response to methanol. CO poisoning is also one of the major issues in current fuel cell technology, so that the catalysts were further exposed to 10% (v/v) CO in oxygen to test their tolerance to CO poisoning effect. Figure 6c shows that the Pt−C catalyst is easily poisoned with a sharp current decrease of ∼50% after CO introduction, whereas the N-HCNPs catalyst is insensitive to CO.

4. CONCLUSIONS

The metal-free N-HCNPs constructed in this study exhibited excellent ORR electrocatalytic activity that approximates that of the commercial Pt−C catalyst. Compared with nitrogen-free HCNPs, the significant improvement in activity for N-HCNPs is probably due to their intrinsic property and can be attributed to the different O_2 adsorption kinetics and reaction pathway derived from the nitrogen-induced effect. In addition, N-HCNPs exhibited better long-term stability and tolerance to methanol crossover and CO poisoning than the Pt−C catalyst in alkaline electrolyte. Our findings suggest that the N-HCNP catalyst is a potential alternative to platinum-based catalysts as efficient and low-cost fuel cell cathodic catalyst.

AUTHOR INFORMATION

Corresponding Author

*Tel: +86-351-4048715. Fax: +86-351-4048433. E-mail: zjh_sx@sxicc.ac.cn (J.Z.), zpzhu@sxicc.ac.cn (Z.Z.).

ACKNOWLEDGMENT

This work was supported by the Natural Science Foundation of China (nos. 20673135 and 50702065), Shanxi Natural Science Foundation (2008021029-1), and the Knowledge Innovation Project of Chinese Academy of Sciences (no. KJCX2.YW.M10).

REFERENCES

(1) Xiong, W.; Du, F.; Liu, Y.; Perez, A.; Supp, M.; Ramakrishnan, T. S.; Dai, L. M.; Jiang, L. *J. Am. Chem. Soc.* **2010**, *132*, 15839–15841.
(2) Chen, Z.; Higgins, D.; Tao, H. S.; Hsu, R. S.; Chen, Z. W. *J. Phys. Chem. C* **2009**, *113*, 21008–21013.
(3) Gong, K.; Du, F.; Xia, Z.; Durstock, M.; Dai, L. *Science* **2009**, *323*, 760–764.
(4) Tominaka, S.; Hayashi, T.; Nakamura, Y.; Osaka, T. *J. Mater. Chem.* **2010**, *20*, 7175.
(5) Thorum, M. S.; Yadav, J.; Gewirth, A. A. *Angew. Chem., Int. Ed.* **2008**, *48*, 165–167.
(6) Lefevre, M.; Proietti, E.; Jaouen, F.; Dodelet, J. P. *Science* **2009**, *324*, 71–74.
(7) Yu, D. S.; Zhang, Q. A.; Dai, L. M. *J. Am. Chem. Soc.* **2010**, *132*, 15127–15129.
(8) Yang, S. Z.; Zhao, G. L.; Khosravi, E. *J. Phys. Chem. C* **2010**, *114*, 3371–3375.
(9) Rao, C. V.; Cabrera, C. R.; Ishikawa, Y. *J. Phys. Chem. Lett.* **2010**, *1*, 2622–2627.
(10) Nagaiah, T. C.; Kundu, S.; Bron, M.; Muhler, M.; Schuhmann, W. *Electrochem. Commun.* **2010**, *12*, 338–341.
(11) Chen, Z.; Higgins, D.; Chen, Z. *Carbon* **2010**, *48*, 3057–3065.
(12) Tang, Y.; Allen, B. L.; Kauffman, D. R.; Star, A. *J. Am. Chem. Soc.* **2009**, *131*, 13200–13201.
(13) Xu, X. A.; Jiang, S. J.; Hu, Z.; Liu, S. Q. *ACS Nano* **2010**, *4*, 4292–4298.
(14) Qu, L. T.; Liu, Y.; Baek, J. B.; Dai, L. M. *ACS Nano* **2010**, *4*, 1321–1326.
(15) Liu, R.; Wu, D.; Feng, X.; Müllen, K. *Angew. Chem., Int. Ed.* **2010**, *49*, 2565–2569.
(16) Jia, R. R.; Chen, J. Z.; Zhao, J. H.; Zheng, J. F.; Song, C.; Li, L.; Zhu, Z. P. *J. Mater. Chem.* **2010**, *20*, 10829–10834.
(17) Song, C.; Du, J. P.; Zhao, J. H.; Feng, S. A.; Du, G. X.; Zhu, Z. P. *Chem. Mater.* **2009**, *21*, 1524–1530.
(18) Chen, Q. D.; Dai, L. M.; Gao, M.; Huang, S. M.; Mau, A. *J. Phys. Chem. B* **2001**, *105*, 618–622.
(19) Kundu, S.; Nagaiah, T. C.; Xia, W.; Wang, Y. M.; Van Dommele, S.; Bitter, J. H.; Santa, M.; Grundmeier, G.; Bron, M.; Schuhmann, W.; Muhler, M. *J. Phys. Chem. C* **2009**, *113*, 14302–14310.
(20) Ikeda, T.; Boero, M.; Huang, S.-F.; Terakura, K.; Oshima, M.; Ozaki, J.-i. *J. Phys. Chem. C* **2008**, *112*, 14706–14709.
(21) Niwa, H.; Horiba, K.; Harada, Y.; Oshima, M.; Ikeda, T.; Terakura, K.; Ozaki, J.-i.; Miyata, S. *J. Power Sources* **2009**, *187*, 93–97.
(22) Chen, W.; Chen, S. W. *Angew. Chem., Int. Ed.* **2009**, *48*, 4386–4389.
(23) Pattabi, M.; Castellanos, R. H.; Castillo, R.; Ocampo, A. L.; Moreira, J.; Sebastian, P. J.; McClure, J. C.; Mathew, X. *Int. J. Hydrogen Energy* **2001**, *26*, 171–174.
(24) Gochi-Ponce, Y.; Alonso-Nunez, G.; Alonso-Vante, N. *Electrochem. Commun.* **2006**, *8*, 1487–1491.
(25) Halseid, R.; Bystron, T.; Tunold, R. *Electrochim. Acta* **2006**, *51*, 2737–2742.
(26) Wakabayashi, N.; Takeichi, M.; Itagaki, M.; Uchida, H.; Watanabe, M. *J. Electroanal. Chem.* **2005**, *574*, 339–346.
(27) Damjanovic, A.; Sepa, D. B. *Electrochim. Acta* **1990**, *35*, 1157–1162.
(28) Paulus, U. A.; Schmidt, T. J.; Gasteiger, H. A.; Behm, R. J. *J. Electroanal. Chem.* **2001**, *495*, 134–145.
(29) Lee, K.-H.; Sinnott, S. B. *Nano Lett.* **2005**, *5*, 793–798.
(30) Mowbray, D.; Morgan, C.; Thygesen, K. *Phys. Rev. B* **2009**, *79*, 195431.

(31) Sorescu, D. C.; Jordan, K. D.; Avouris, P. *J. Phys. Chem. B* **2001**, *105*, 11227–11232.
(32) Ulbricht, H.; Moos, G.; Hertel, T. *Phys. Rev. B* **2002**, *66*, 075404.
(33) Hu, X. B.; Wu, Y. T.; Li, H. R.; Zhang, Z. B. *J. Phys. Chem. C* **2010**, *114*, 9603–9607.
(34) Shan, B.; Cho, K. *Chem. Phys. Lett.* **2010**, *492*, 131–136.